Earth and Planetary Science Letters 406 (2014) 7–13

Contents lists available at ScienceDirect

Earth and Planetary Science Letters

www.elsevier.com/locate/epsl

Seismic versus aseismic slip: Probing mechanical properties of the northeast Japan subduction zone

M. Shirzaei [a,*], R. Bürgmann [b], N. Uchida [c], Y. Hu [b], F. Pollitz [d], T. Matsuzawa [c]

[a] School of Earth and Space Exploration, Arizona State University, Tempe, AZ, USA
[b] Department of Earth and Planetary Science, University of California, Berkeley, CA, USA
[c] Graduate School of Science, Tohoku University, Sendai, Japan
[d] U.S. Geological Survey, Menlo Park, CA, USA

ARTICLE INFO

Article history:
Received 14 May 2014
Received in revised form 25 August 2014
Accepted 27 August 2014
Available online xxxx
Editor: P. Shearer

Keywords:
postseismic deformation
Tohoku earthquake
rate state friction law

ABSTRACT

Fault slip may involve slow aseismic creep and fast seismic rupture, radiating seismic waves manifested as earthquakes. These two complementary behaviors accommodate the long-term plate convergence of major subduction zones and are attributed to fault frictional properties. It is conventionally assumed that zones capable of seismic rupture on the subduction megathrust are confined to between about 10 to 50 km depth; however, the actual spatiotemporal distribution of fault mechanical parameters remains elusive for most subduction zones. The 2011 Tohoku M_w 9.0 earthquake ruptured with >50 m slip up to the trench, thus challenging this conventional assumption, and provides a unique opportunity to probe the mechanical properties of the Japan subduction zone. Drawing on the inferred distribution of coseismic and postseismic slip, it has recently been suggested that portions of the megathrust are capable of switching between seismic and aseismic behavior. Kinematic models of the coseismic rupture and 15-month postseismic afterslip of this event suggest that the coseismic rupture triggered widespread frictional afterslip with equivalent moment magnitude of 8.17–8.53, in addition to viscoelastic relaxation in the underlying mantle. The identified linear relation between modeled afterslip, slip inferred from repeating earthquakes on the plate interface, and the cumulative number of aftershocks within 15 km distance of the subduction thrust suggests that most aftershocks are a direct result of afterslip. We constrain heterogeneous rate-state friction parameters of the subduction thrust from the computed coseismic stress changes and afterslip response. Our results indicate a variable pattern along dip and strike, characterizing areas down-dip and south of the main rupture zone as having velocity-strengthening properties. In agreement with seismic tomographic models of plate boundary elastic properties and geologic evidence for previous M > 8.5 megathrust earthquakes on this section of the plate boundary, we suggest that the obtained pattern of the frictional properties is characteristic of subducted material and thus persistent in time and space.

1. Introduction

Fault slip comprises seismic and aseismic components, which occur on patches with velocity weakening (VW) and velocity strengthening (VS) properties (Dieterich, 1978; Ruina, 1983), respectively. Traditionally, it is thought that VW properties characterize the depth range of 10 to 50 km on subduction zones, governed by material properties, fluid pressure and temperature (Pacheco et al., 1993). However, identifying the actual distribution and temporal evolution of patchworks of VW and VS behavior has proven challenging (Barbot et al., 2009; Perfettini et al., 2010; Shirzaei et al., 2013). For instance, portions of a fault that exhibit longer-term VS behavior, undergoing stable creep at low velocities comparable to tectonic rates, may alter their frictional behavior to VW (Noda and Lapusta, 2013; Reinen et al., 1991; Shibazaki et al., 2011) and experience fast dynamic rupture with slip rates of order of 1 m/s due to dynamic weakening effects (Noda and Lapusta, 2013). Moreover, the zones that are effectively locked during the interseismic period may contain patches of VS behavior slipping at low rates, which are held back by surrounding locked VW zones (Bürgmann et al., 2005). It has also been suggested that areas that previously ruptured in M 7–8 ruptures in the northeast Japan subduction zone slipped stably following the Tohoku earthquake (Johnson et al., 2012). Thus identifying the spatial extent and temporal evolution of VW and VS properties on the

* Corresponding author. Tel.: +1 480 727 4193; fax: +1 480 965 8102.
E-mail address: Shirzaei@asu.edu (M. Shirzaei).

http://dx.doi.org/10.1016/j.epsl.2014.08.035
0012-821X/

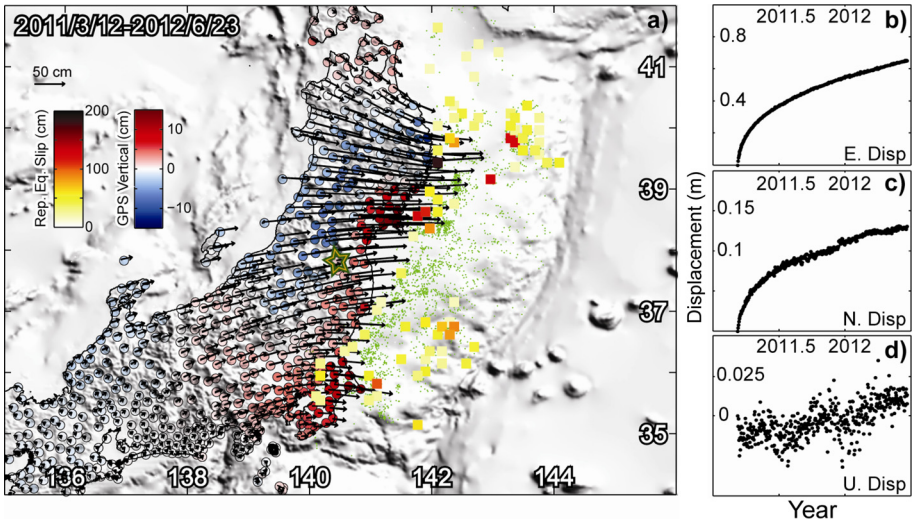

Fig. 1. (a) The cumulative 3D surface deformation measured with continuous GPS observations during 15-month postseismic period (arrows and colored circles onshore) [source: Geospatial Information Authority of Japan]. The distribution of aftershocks during this period is shown by green dots [source: F-net Japan broadband seismograph network]. The colored squares offshore indicate groups of repeating earthquakes (Uchida and Matsuzawa, 2013). Each circle is color-coded by the equivalent cumulative postseismic creep from 3 days after the mainshock through June 23, 2012, (b–d) examples of time series of the 3D postseismic displacement at a selected GPS station, marked by green star in panel (a), eastward and northward displacements are considered as positive. (For interpretation of the references to color in this figure legend, the reader is referred to the web version of this article.)

off-Tohoku subduction zone is of great importance for studying the mechanics of the megathrust and its seismic potential.

The M_w 9.0 Tohoku earthquake occurred on March 11, 2011 on the megathrust where the Pacific plate subducts west-northwestward under the Okhotsk plate at an average rate of ~8 cm/yr (Apel et al., 2006). An important aspect of the rupture models of this event is that slip of ~50 m occurred in the shallowest sections of the subduction zone near the Japan trench (Fig. S1), confirmed by repeated bathymetric (Fujiwara et al., 2011) and seismic reflection data showing large offsets up to the trench (Kodaira et al., 2012). This unexpected large shallow slip caused a destructive large tsunami (Simons et al., 2011) and surprised the scientific community and authorities (Sagiya et al., 2011). This extraordinary behavior is rooted in the particular mechanical properties characterizing the zones of VW and VS behavior (Dieterich, 1978; Ruina, 1983).

The co- and postseismic observations of the deformation associated with this event, provide a unique opportunity to study the spatiotemporal distribution of fault mechanical parameters in a seismically active region (Johnson et al., 2012; Ozawa et al., 2012, 2011; Pollitz et al., 2011; Simons et al., 2011). The postseismic deformation, driven by the stress imparted during coseismic rupture (Bürgmann and Dresen, 2008), comprises afterslip on the megathrust, viscoelastic relaxation of the volume surrounding the fault and poroelastic rebound. Here, we investigate Global Positioning System (GPS) time series spanning the first 15 months of the surface deformation following the event (Fig. 1), complemented with direct observation of the creep on the megathrust interface obtained using characteristic repeating earthquakes (CREs) (Uchida and Matsuzawa, 2013). The combination of these two data sets allows us to illuminate the kinematics of the afterslip and probe the spatial distribution of rate-state frictional properties on the subduction plate interface of NE Japan.

2. Data

The co- and postseismic observations of the 3D deformation associated with the Tohoku earthquake are recorded at more than 1000 continuous and campaign GPS stations (Ozawa et al., 2012). The GPS time series are provided by the Geospatial Information Authority of Japan. Here, we focus on the cumulative 3D surface deformation measured during the initial 15-month postseismic period (see Fig. 1 and supplementary movies). The postseismic GPS time series (Ozawa et al., 2012) are characterized by a rapidly decaying pattern seen in postseismic deformation elsewhere (Bürgmann and Dresen, 2008; Hsu et al., 2006; Perfettini and Avouac, 2007). The vertical deformation shows zones of uplift along the Pacific coast, whereas the far coast is characterized by subsidence (Fig. 1a).

We also explore characteristic repeating earthquakes (CREs). The CREs are events on the plate interface that have nearly identical waveforms and that have coincident hypocenters to resolutions of a few 10s of meters (Uchida and Matsuzawa, 2013). Because of these attributes, a time-ordered sequence of repeating events is believed to represent repeated failures of the same small fault patch, loaded by aseismic slip on the surrounding fault surface (Nadeau and Johnson, 1998; Schaff et al., 1998). Events in a group of CREs have recurrence intervals that generally vary in proportion to the inverse of the creep rate on the fault where the repeating earthquakes are located, indicating that they act as creepmeters directly installed on the fault interface. Thus, the location, magnitude and recurrence interval properties of the sequences can be used to infer the spatial and temporal distribution of deep aseismic slip (Nadeau and Johnson, 1998; Schaff et al., 1998). The cumulative slip obtained from post-Tohoku earthquake measurements of CREs (Fig. 1a) indicates no resolvable afterslip within the primary co-seismic rupture area and that the inferred postseismic creep surrounds the coseismic rupture and exhibits a temporal decay similar to that seen in the GPS data (Uchida and Matsuzawa, 2013).

3. Time-dependent afterslip model

To model the postseismic deformation of the first 15 months we consider three scenarios (Fig. 2), assuming the observed deformation resulted from afterslip on the subduction thrust fault buried in an elastic half-space medium and; (a) no viscoelastic relaxation is involved, (b) the viscoelastic relaxation occurs in a layered viscoelastic medium, (c) the viscoelastic relaxation occurs in a 3D layered viscoelastic medium that includes an elastic slab and higher-viscosity mantle below the Pacific-plate lithosphere. In the latter two cases, the optimum contribution

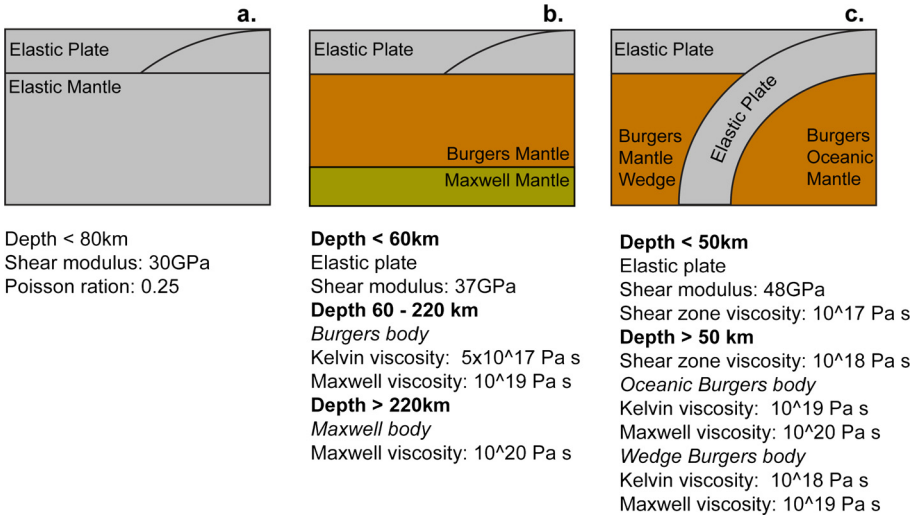

Fig. 2. Three different scenarios used for modeling the postseismic deformation. (a) Afterslip on a thrust fault buried in an elastic half-space medium and with no viscoelastic relaxation involved, (b) afterslip on a thrust fault buried in an elastic half-space and viscoelastic relaxation in a layered viscoelastic medium using model parameters of Pollitz et al. (2006), (c) afterslip on a thrust fault buried in an elastic half-space medium the viscoelastic relaxation occurs in a three-dimensional viscoelastic medium that includes an elastic slab and higher-viscosity oceanic mantle using model parameters of Hu and Wang (2012).

of the viscoelastic relaxation is estimated during the afterslip inversion as described below. Additional viscoelastic relaxation driven by the afterslip is not considered. The viscoelastic parameters of the forward models used for this correction were adopted from those obtained in prior investigations of postseismic deformation of the 2004 Sumatra earthquake (Hu and Wang, 2012; Pollitz et al., 2006), which are consistent with the values found for other large subduction zone events (Wang et al., 2012). The viscoelastic model used in scenario (b) is produced using the Visco1D software (http://earthquake.usgs.gov/research/software/#VISCO1D; Pollitz, 1997) and that of scenario (c) is generated using a 3D finite element code developed by Hu et al. (2004).

The plate interface that the afterslip occurs on extends from 10 km to 80 km depth, has variable dip and strike (Fig. S2), and is defined using a combination of various seismic data sets (Hayes et al., 2012). The same geometry is used for modeling the coseismic slip. In the coseismic and afterslip model inversions, the elastic half-space is characterized by a Poisson's ratio of 0.25 and shear modulus of 30 GPa. To associate the daily time series of surface displacement with the kinematics of the spatiotemporal distribution of the afterslip, we implement a time-dependent inverse modeling scheme (Shirzaei and Bürgmann, 2013). This method consists of two main operators; (1) a robust optimization operator using the L1-norm minimization as a minimum spatial mean error estimator (Marshall and Bethel, 1996), and (2) a linear Kalman filter (LKF) (Grewal and Andrews, 2001) to generate the time series of the afterslip for each triangular dislocation of the fault-interface mesh as a minimum temporal mean square error estimator. These two steps are implemented iteratively (Shirzaei and Walter, 2010). At each time step t, the mathematical relation between surface observation (L_t) and afterslip (S_t) is as follows:

$$L_t + v_t = BS_t + \alpha V_E, \qquad P_t = \sigma_0^2 \Sigma_{l_t l_t}^{-1}$$
$$l_b \le S_t \le u_b, \quad t = 1, 2, 3, \ldots, N, \; 0 < \alpha < 2 \tag{1}$$

where $L_t = [l_t(x_1, y_1), l_t(x_2, y_2), \ldots, l_t(x_n, y_n)]^T$ is the time series of the observed surface displacement at n GPS stations with surface locations of $\{(x_i, y_i)\}_{i=1:n}$, $S_t = \{s_t(\omega_1, \rho_1), s_t(\omega_2, \rho_2), \ldots, s_t(\omega_m, \rho_m)\}$ is the time series of afterslip at a patch located at $\{(\omega_i, \rho_i)\}_{i=1:m}$ along strike and dip of the slab (Fig. S2), B is the design matrix that includes Green's functions relating fault dislocation to the surface displacements, V_E is the contribution from viscoelastic relaxation of the upper mantle and lower crust for scenarios b and c, $\propto$ is the scaling factor of the viscoelastic deformation, v_t is the vector of observation residuals, $\Sigma_{l_t l_t}$ is the variance covariance matrix of the observations, and σ_0^2 is the reference variance factor, initially considered to be one (Mikhail, 1976). Before solving for the time-dependent kinematic model of the afterslip, the time series of V_E is obtained through forward modeling using the scenarios shown in Fig. 2b, c. The scaling factor (α) of the viscoelastic model deformation is jointly estimated during the slip inversion. Fig. S3 shows the 15-month cumulative 3D surface displacements due to the viscoelastic relaxation associated with scenarios b and c before scaling by their respective α factors. The scaling factor is considered because the chosen values of the viscosity structure used for forward modeling (Hu and Wang, 2012; Pollitz et al., 2006) may not be representative for this study area, thus the factor allows optimizing the initial value of the viscosity and thus the deformation contribution from the viscoelastic model. To integrate the CREs into the afterslip inversion, we consider the following equations:

$$S_t^{CRE} + \varepsilon_t = S_t, \qquad P_t^c = \sigma_0^2 \Sigma_{S_t S_t}^{-1} \tag{2}$$

where, S_t^{CRE} is the slip obtained from the CREs, ε_t is the vector of observation residuals and P_t^c is the weight matrix.

To obtain an optimum afterslip model, Eqs. (1) and (2) are solved jointly subject to an objective function, the L1-norm of the observation residuals as follows:

$$\left\| \begin{bmatrix} P_t & 0 \\ 0 & P_t^c \end{bmatrix} \begin{bmatrix} v_t \\ \varepsilon_t \end{bmatrix} \right\|_{L1} \rightarrow \min \tag{3}$$

To reduce the roughness of the slip distribution on the fault plane and avoid unrealistic stress heterogeneities, we minimize the second-order derivative of the afterslip as an additional constraint (e.g., Segall and Harris, 1987).

$$\gamma D S_t = 0 \tag{4}$$

where, D is the Laplacian operator and γ is the smoothing factor, which determines the roughness of the optimum creep model. Here, we constrain afterslip to be dip-slip only and apply a zero-slip constraint to the southern and northern edges of the fault mesh.

Following optimizing the afterslip model for all observation times $\{t_1, t_2, \ldots, t_N\}$ and determining the time series of the slip

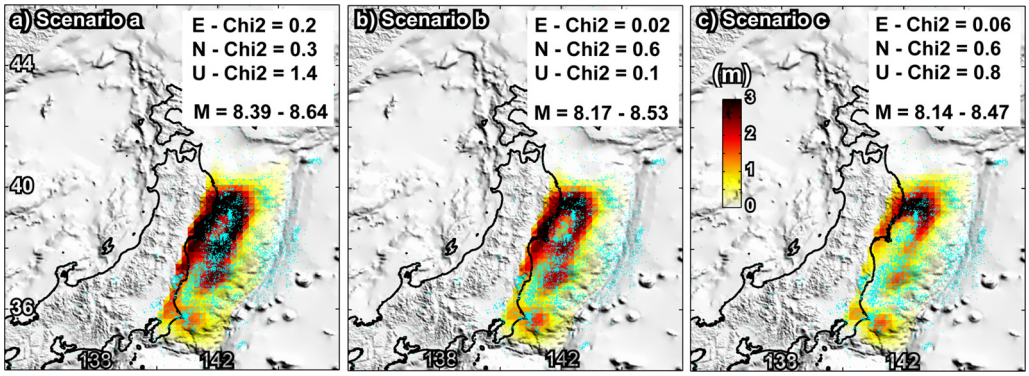

Fig. 3. The cumulative afterslip model of the first 15 months associated with the three scenarios. (a) Scenario a, no viscoelastic relaxation is considered. (b) Scenario b, the viscoelastic relaxation resulting from model shown in Figs. 2b and S3a is scaled by a factor of 0.7 ± 0.1. (c) Scenario c, the viscoelastic relaxation resulting from model shown in Fig. 2c and S3b is scaled by a factor of 0.9 ± 0.2. For each scenario the estimated 15-month afterslip moment release and the value of the Chi-square misfit statistic for three components of the GPS observations are provided. The distribution of the aftershocks during this period is shown by cyan dots.
Source: F-net Japan broadband seismograph network.

and the associated variance–covariance for each patch, we apply the LKF to reduce temporal noise. The LKF addresses the problem of estimating the parameters of a linear, stochastic system with measurements that are linear functions of the parameters. Given the time series of slip $\{s_1, ..., s_N\}$ for a patch located at (ω_j, ρ_j) and the associated variance of $\{\delta_1^2, ..., \delta_N^2\}$, according to the original form of the LKF, the system dynamics and measurement models, respectively, are:

$$S_i = \begin{bmatrix} V_l & 1 \end{bmatrix} \begin{bmatrix} t_i - t_{i-1} \\ S_{i-1} \end{bmatrix} + q_{i-1}, \quad q_i \sim N(0, Q)$$
$$S_i = S_i + r_i, \quad r_i \sim N(0, R) \tag{5}$$

where q_i, q and r_i are Gaussian-distributed noise with mean value of 0 and standard deviation of $1/N \sum_{j=1}^{N} \delta_j$ and V_l is the linear slip velocity. A recursive solution for the system of Eqs. (5) is provided by Grewal and Andrews (2001). In the next section, we describe the results of applying this inversion scheme to the 15-month time series of the surface deformation and CRE data.

4. Results

We start with modeling the coseismic rupture using the GPS data. To obtain the coseismic displacements we difference the daily GPS solutions from one day before and one day after the event. Thus, the coseismic signal includes the effect of both the mainshock and an M_w 7.9 aftershock that occurred 30 min later. The inverted coseismic slip model is shown in Fig. S1 and is very similar to rupture models obtained in other studies (Iinuma et al., 2012; Ozawa et al., 2012; Pollitz et al., 2011; Simons et al., 2011). The model has a primary high-slip zone with ~50 m of slip near the trench separated by a zone of negligible slip from a deeper locus at ~35 km depth.

In the following and to obtain the time-dependent afterslip model explaining the 3D GPS and CRE time series, we test the three scenarios mentioned above and estimate the model misfits as a function of time. Fig. 3 provide the distribution of the cumulative afterslip model for the three scenarios, the associated chi-square reduction and the standard deviation of the misfit to the repeating earthquake data. Fig. S5 shows the time series of the standard deviation of misfits for the 15 months postseismic period. Models developed according to the three scenarios explain the horizontal GPS deformation data well. In scenario b, with a scaling factor of the viscoelastic model contribution $\alpha = 0.7 \pm 0.1$, the standard deviation of the misfit to the GPS vertical components is smaller by a factor of 2–3 than in the others. The scaling factor of the viscoelastic model contribution for scenario c is $\alpha = 0.9 \pm 0.2$. The afterslip model obtained in scenario b yields a somewhat better fit to the repeating earthquakes compared to scenario a, while scenario b and c explain the CRE data equally well (Fig. S5). Here we focus on the afterslip obtained through scenario b and we base the rest of analysis on it.

In the best-fitting afterslip models obtained in scenario b (Fig. 4a, Figs. S4–5 and supplementary movies), the slip occurs primarily down-dip of the coseismic rupture. While the general pattern remains stationary through time (supplementary movie showing the evolution of afterslip), the inverted slip distribution varies along dip and strike of the subduction zone. We find a maximum cumulative afterslip of ~3.5 m to the north of the coseismic rupture at a depth of 35–50 km. The amplitude of the slip decreases toward the south of the coseismic rupture. Sensitivity tests (Fig. S6) show that using a combination of CREs with 3D GPS data improves the slip resolution and highlights the complementary nature of these data sets. Fig. 4b–d shows that the inverted afterslip model agrees well with the slip measured using CREs, but the CRE data suggest that slip is locally more heterogeneous than is resolvable in the inversion. Within 1σ uncertainly of the model inversion and assuming a shear modulus of 30 GPa in scenario b, the estimated 15-month afterslip reflects a moment release of 2.30×10^{21}–7.9×10^{21} N m equivalent to $M_w = 8.17$–8.53, corresponding to 6–20% of the coseismic moment release (see also supplementary movies). This result is comparable to other estimates of the megathrust afterslip moment release during similar time periods for other subduction earthquakes (Hsu et al., 2006; Savage et al., 2007). The seismic moment released by earthquakes $M_w \geq 4$ detected by F-net (Japan broadband seismograph network) during the same period corresponds to a moment of 2.01×10^{20} N m, so about 96% of the postseismic slip was aseismic.

5. Discussion

The cumulative afterslip model (Fig. 3 and supplement movies) suggests that co- and postseismic slip are complementary and the slight overlap is likely due to the smoothing operator used and inherent resolution limits (Evans and Meade, 2012). To further investigate this complementary nature, we consider the pattern of the Coulomb failure stress change (ΔCFS) induced by the coseismic rupture on the megathrust (see supplementary materials). We find a significant correlation between areas of increased ΔCFS and the zone of afterslip, suggesting that the afterslip is a direct response to the stress imparted during the coseismic rupture.

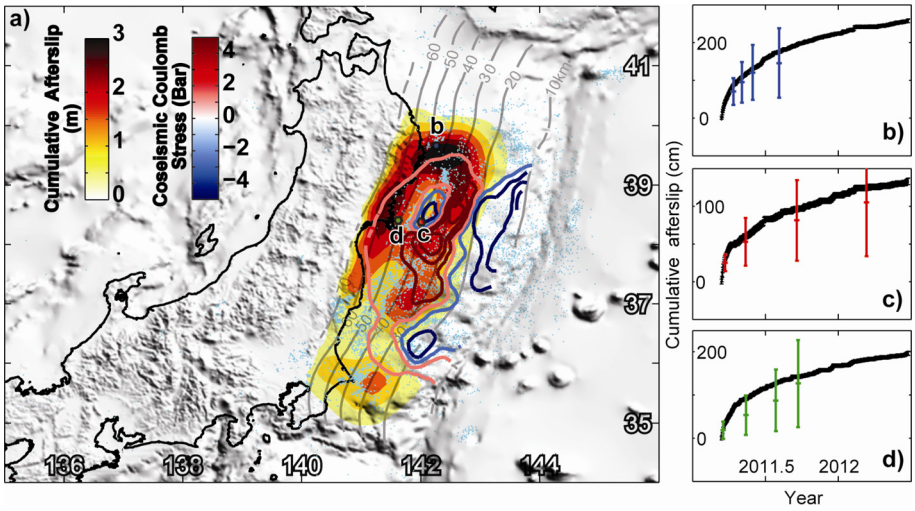

Fig. 4. (a) Spatial distribution of the cumulative afterslip obtained from joint inversion of 3D GPS data and time series of repeating earthquake slip corrected for visco-elastic relaxation in a layered Earth model (Fig. 2b). Overlaid contours represent the imparted Coulomb failure stress change on the megathrust due to the Tohoku event. (b–d) Examples of time series of the inverted afterslip and the creep obtained from repeating earthquakes. The locations of the corresponding repeater sequences are marked in panel (a). The error bars on the CRE time series represent ±50% of their actual values. The afterslip models for all three scenarios are shown in Fig. 3.

Given the pattern of the repeating earthquakes and assuming that the majority of aftershocks occur on the fault interface in areas surrounding the coseismic rupture (Asano et al., 2011), we want to test whether the evolution of aftershocks might be governed by the afterslip. To this end we investigate the correlation between cumulative number of aftershocks and the afterslip time series. Fig. 4b shows a bivariate plot relating time series of the cumulative afterslip at the patch of maximum afterslip to the corresponding cumulative number of aftershocks within a 35×35 km^2 area around that patch. The linear relation exhibited in the plot suggests that both afterslip and aftershocks follow the same temporal pattern and thus the evolution of aftershocks is linked to afterslip driven by the coseismic stress changes. A similar relation has been observed elsewhere (Hsu et al., 2006). Closer to the trench, where the distance of the aftershocks to the slab increases (Fig. 4a), the linear relation weakens (Fig. 4c, d). Here the aftershocks are widely scattered in the volume surrounding the zone of the primary rupture asperity, diverse focal mechanisms show that the aftershocks are dominantly off-fault (Asano et al., 2011), the inferred afterslip is small, and aftershocks do not follow a simple relation with the inferred afterslip.

Using the afterslip model and the coseismic Coulomb failure stress change (ΔCFS), we are able to estimate the fault mechanical parameter (A). This parameter represents the direct effect of increase of friction with log of velocity increase in rate-state friction framework for velocity-strengthening aseismic fault slip. Given the long term slip rate (V_0) and the afterslip velocity (V_a) directly following the main shock, we use the following relation (Perfettini et al., 2010):

$$A = \Delta CFS / \log(V_a / V_0) \tag{6}$$

Large values of A is an indicator for strong VS properties. Using the ΔCFS shown in Fig. 4 and estimate of V_a from the first 4 days of afterslip (Fig. S7), we obtain the spatial distribution of A as shown in Fig. 6a. The values of A at the zone of maximum afterslip range between 0.2 and 0.5 MPa, similar to values found in previous studies (Perfettini et al., 2010). Moreover, in the zone of maximum afterslip as shown in Fig. 6b, the inverted afterslip model is reproduced well using $U(t) = V_0 t_r \ln[(V_a/V_0 t_r)t + 1]$, predicted from rate-strengthening frictional sliding, assuming that frictional stress increases linearly with the logarithm of the sliding velocity and that the contributions from ongoing plate convergence and viscous relaxation are negligible (Marone, 1998). Given the $V_0 = 8$ cm/yr, the relaxation time (t_r) is estimated to be between 7.9 and 10.3 yrs.

The distribution of A indicates a complex pattern along the strike and dip of the megathrust. The identified zones of VS afterslip appear to coincide with zones of low P-wave velocities determined by seismic tomography (Zhao et al., 2011) (Fig. 5), suggesting material properties may control the fault frictional properties. The low velocity zones may be associated with serpentinization of the mantle wedge, subducted sediments and increased fluid pressure and as a result the subduction zone becomes decoupled (or weakly coupled) (Zhao et al., 2011) over the zones of low velocities.

Sediment analysis and hydrodynamic simulations indicate that the northeastern coast of Japan was repeatedly invaded by the tsunamis inferred to be due to Tohoku-size earthquakes (Minoura et al., 2005, 2001; Sawai et al., 2008). The average recurrence interval of these tsunamis is estimated to be ~1000 yrs (Minoura et al., 2001). The geological evidence and model simulations suggest that during the past several thousand years, earthquakes comparable in size and location to the Tohoku event have ruptured similar part of the subduction zone. These long term evidences in conjunction with the distribution of the frictional properties and the mechanical composition of the subduction zone, favors zones with persistent VW vs VS properties.

6. Conclusions

We investigated 15-month postseismic deformation associated with Tohoku earthquake. We found that a most of the postseismic deformation data can be explained using a combination of frictional afterslip and viscoelastic relaxation of the upper mantle and lower crust. The estimated 15-month afterslip reflects a moment release of 2.30×10^{21}–7.9×10^{21} N m equivalent to $M_w = 8.17$–8.53. The correlation between areas of increased ΔCFS and zone of afterslip, suggests that the afterslip is a direct response to the stress imparted during the coseismic rupture. Using rate-state friction law, we estimated the fault mechanical properties, assuming that the patches of high afterslip are characterized by velocity strengthening properties. The presented observations and models suggest that the estimated mechanical properties are likely to be persistent in time and space and thus Tohoku-size earth-

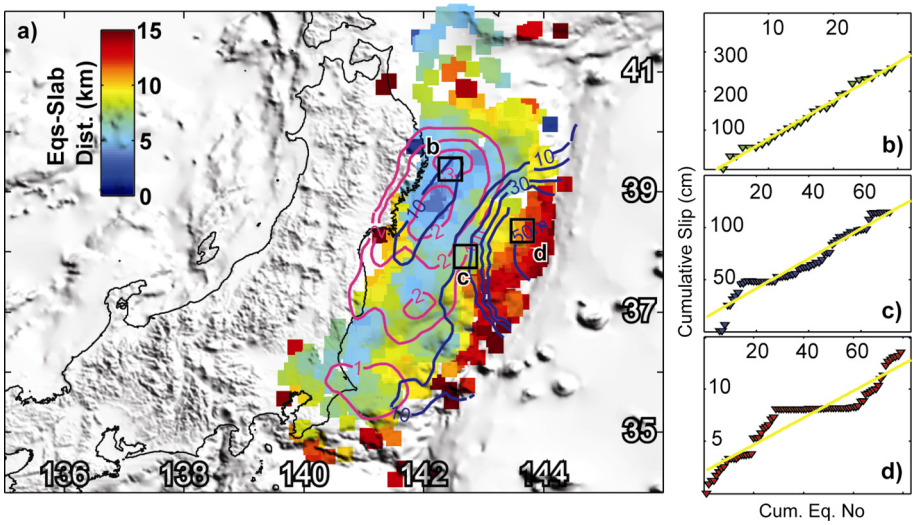

Fig. 5. (a) Shows the spatial distribution and mean distance of the aftershocks from the plate interface. Here only events within 15 km from the slab are considered. The contour lines indicate the inverted slip of the coseismic rupture (blue lines) and 15-month cumulative afterslip (magenta). Contours are in meters. (b–d) Bivariate plots showing the mutual relation between afterslip time series and cumulative number of aftershocks within 15 km of the subduction thrust in a 35 km × 35 km box at selected areas shown in panel (a). (For interpretation of the references to color in this figure legend, the reader is referred to the web version of this article.)

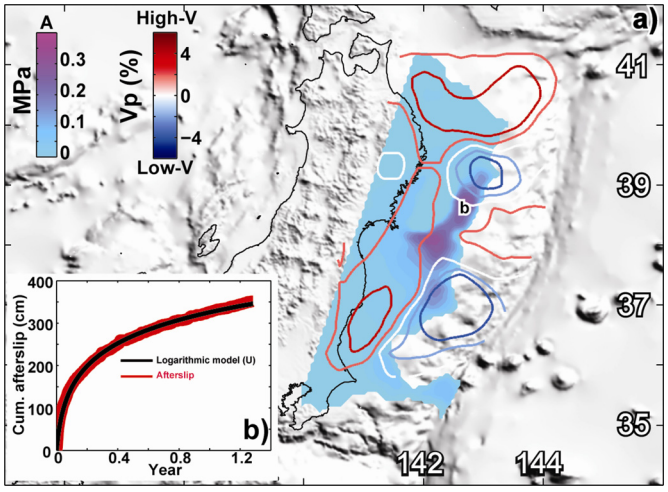

Fig. 6. (a) Fault mechanical parameter. The filled color contours shows the spatial distribution of the rate-state frictional parameter A indicating zones of variable velocity strengthening. The contour lines with blue–white–red colorbar show the P-wave tomography in the megathrust zone (Zhao et al., 2011). Red indicates zones of high seismic velocity (V_p), while blue is associated with zones of low velocity. (b) Shows the modeled cumulative afterslip (red) obtained at the location marked by letter b in panel (a) versus theoretical displacements (black) given by equation $U(t) = V_0 t_r \ln[(V_a/V_0 t_r)t + 1]$ predicted from rate-strengthening frictional sliding, which assumes that frictional stress increases linearly with the logarithm of the sliding velocity (Marone, 1998). In this equation, $U(t)$ is the cumulative afterslip. Given $V_0 = 8\frac{\text{cm}}{\text{yr}}$, the relaxation time t_r is estimated to be between 7.9 and 10.3 yrs at this location. (For interpretation of the references to color in this figure legend, the reader is referred to the web version of this article.)

quakes have ruptured similar part of the subduction zone and will do so again.

Appendix A. Supplementary material

Supplementary material related to this article can be found online at http://dx.doi.org/10.1016/j.epsl.2014.08.035.

References

Apel, E.V., Bürgmann, R., Steblov, G., Vasilenko, N., King, R., Prytkov, A., 2006. Independent active microplate tectonics of northeast Asia from GPS velocities and block modeling. Geophys. Res. Lett. 33 (11).

Asano, Y., Saito, T., Ito, Y., Shiomi, K., Hirose, H., Matsumoto, T., Aoi, S., Hori, S., Sekiguchi, S., 2011. Spatial distribution and focal mechanisms of aftershocks of the 2011 off the Pacific coast of Tohoku Earthquake. Earth Planets Space 63 (7), 669–673.

Barbot, S., Fialko, Y., Bock, Y., 2009. Postseismic deformation due to the Mw 6.0 2004 Parkfield earthquake: stress-driven creep on a fault with spatially variable rate-and-state friction parameters. J. Geophys. Res. 114, B07405. http://dx.doi.org/10.1029/2008JB005748.

Bürgmann, R., Dresen, G., 2008. Rheology of the lower crust and upper mantle: evidence from rock mechanics, geodesy, and field observations. In: Annual Review of Earth and Planetary Sciences. Annual Reviews, Palo Alto. Annu. Rev. Earth Planet. Sci., 531–567.

Bürgmann, R., Kogan, M.G., Steblov, G.M., Hilley, G., Levin, V.E., Apel, E., 2005. Interseismic coupling and asperity distribution along the Kamchatka subduction zone. J. Geophys. Res. 110 (B7).

Dieterich, J.H., 1978. Time-dependent friction and the mechanics of stick slip. Pure Appl. Geophys. 116, 790–806.

Evans, E.L., Meade, B.J., 2012. Geodetic imaging of coseismic slip and postseismic afterslip: sparsity promoting methods applied to the great Tohoku earthquake. Geophys. Res. Lett. 39.

Fujiwara, T., Kodaira, S., No, T., Kaiho, Y., Takahashi, N., Kaneda, Y., 2011. The 2011 Tohoku–Oki earthquake: displacement reaching the trench axis. Science 334 (6060), 1240.

Grewal, M.S., Andrews, A.P., 2001. Kalman Filtering: Theory and Practice Using MATLAB. Wiley-Interscience. 416 pp.

Hayes, G.P., Wald, D.J., Johnson, R.L., 2012. Slab1.0: a three-dimensional model of global subduction zone geometries. J. Geophys. Res., Solid Earth 117 (B1), B01302.

Hsu, Y.J., Simons, M., Avouac, J.P., Galetzka, J., Sieh, K., Chlieh, M., Natawidjaja, D., Prawirodirdjo, L., Bock, Y., 2006. Frictional afterslip following the 2005 Nias–Simeulue earthquake, Sumatra. Science 312 (5782), 1921–1926.

Hu, Y., Wang, K.L., 2012. Spherical-Earth finite element model of short-term postseismic deformation following the 2004 Sumatra earthquake. J. Geophys. Res., Solid Earth 117.

Hu, Y., Wang, K., He, J., Klotz, J., Khazaradze, G., 2004. Three-dimensional viscoelastic finite element model for postseismic deformation of the great 1960 Chile earthquake. J. Geophys. Res., Solid Earth 109 (B12).

Iinuma, T., Hino, R., Kido, M., Inazu, D., Osada, Y., Ito, Y., Ohzono, M., Tsushima, H., Suzuki, S., Fujimoto, H., Miura, S., 2012. Coseismic slip distribution of the 2011 off the Pacific Coast of Tohoku Earthquake (M9.0) refined by means of seafloor geodetic data. J. Geophys. Res. 117 (B7).

Johnson, K.M., Fukuda, J.i., Segall, P., 2012. Challenging the rate-state asperity model: afterslip following the 2011 M9 Tohoku-oki, Japan, earthquake. Geophys. Res. Lett. 39 (20).

Kodaira, S., No, T., Nakamura, Y., Fujiwara, T., Kaiho, Y., Miura, S., Takahashi, N., Kaneda, Y., Taira, A., 2012. Coseismic fault rupture at the trench axis during the 2011 Tohoku-oki earthquake. Nat. Geosci. 5 (9), 646–650.

Marone, C., 1998. Laboratory-derived friction laws and their application to seismic faulting. Annu. Rev. Earth Planet. Sci. 26, 643–696.

Marshall, J., Bethel, J., 1996. Basic concepts of L1 norm minimization for surveying applications. J. Surv. Eng. 122 (4), 168–179.

Mikhail, E.M., 1976. Observations and Least Squares. IEP, New York. 497 pp.
Minoura, K., Imamura, F., Sugawara, D., Kono, Y., Iwashita, 2001. The 869 Jogan tsunami deposit and recurrence interval of large-scale tsunami on the Pacific coast of northeast Japan. J. Nat. Disaster Sci. 23, 83–88.
Minoura, K., Imamura, F., Kuran, U., Nakamura, T., Papadopoulos, G.A., Sugawara, D., Takahashi, T., Yalciner, A.C., 2005. A tsunami generated by a possible submarine slide: evidence for slope failure triggered by the North Anatolian fault movement. Nat. Hazards 36 (3), 297–306.
Nadeau, R.M., Johnson, L.R., 1998. Seismological studies at Parkfield VI: moment release rates and estimates of source parameters for small repeating earthquakes. Bull. Seismol. Soc. Am. 88 (3), 790–814.
Noda, H., Lapusta, N., 2013. Stable creeping fault segments can become destructive as a result of dynamic weakening. Nature 493 (7433), 518.
Ozawa, S., Nishimura, T., Suito, H., Kobayashi, T., Tobita, M., Imakiire, T., 2011. Coseismic and postseismic slip of the 2011 magnitude-9 Tohoku-Oki earthquake. Nature 475 (7356), 373–376.
Ozawa, S., Nishimura, T., Munekane, H., Suito, H., Kobayashi, T., Tobita, M., Imakiire, T., 2012. Preceding, coseismic, and postseismic slips of the 2011 Tohoku earthquake, Japan. J. Geophys. Res. 117 (B7).
Pacheco, J.F., Sykes, L.R., Scholz, C.H., 1993. Nature of seismic coupling along simple plate boundaries of the subduction type. J. Geophys. Res., Solid Earth 98 (B8), 14133–14159.
Perfettini, H., Avouac, J.P., 2007. Modeling afterslip and aftershocks following the 1992 Landers earthquake. J. Geophys. Res. 112 (B7).
Perfettini, H., Avouac, J.P., Tavera, H., Kositsky, A., Nocquet, J.M., Bondoux, F., Chlieh, M., Sladen, A., Audin, L., Farber, D.L., Soler, P., 2010. Seismic and aseismic slip on the central Peru megathrust. Nature 465 (7294), 78–81.
Pollitz, F.F., 1997. Gravitational-viscoelastic postseismic relaxation on a layered spherical Earth. J. Geophys. Res. 102, 17,921–17,941. http://dx.doi.org/10.1029/97JB01277.
Pollitz, F.F., Burgmann, R., Banerjee, P., 2006. Post-seismic relaxation following the great 2004 Sumatra–Andaman earthquake on a compressible self-gravitating Earth. Geophys. J. Int. 167 (1), 397–420.
Pollitz, F.F., Bürgmann, R., Banerjee, P., 2011. Geodetic slip model of the 2011 M9.0 Tohoku earthquake. Geophys. Res. Lett. 38 (7).
Reinen, L.A., Weeks, J.D., Tullis, T.E., 1991. The frictional behavior of serpentinite – implications for aseismic creep on shallow crustal faults. Geophys. Res. Lett. 18 (10), 1921–1924.
Ruina, A., 1983. Slip instability and state variable friction laws. J. Geophys. Res. 88 (B12), 10359–10370.
Sagiya, T., Kanamori, H., Yagi, Y., Yamada, M., Mori, J., 2011. Rebuilding seismology. Nature 473 (7346), 146–148.
Savage, J.C., Svarc, J.L., Yu, S.B., 2007. Postseismic relaxation and aftershocks. J. Geophys. Res., Solid Earth 112 (B6).
Sawai, Y., Fujii, Y., Fujiwara, O., Kamataki, T., Komatsubara, J., Okamura, Y., Satake, K., Shishikura, M., 2008. Marine incursions of the past 1500 years and evidence of tsunamis at Suijin-numa, a coastal lake facing the Japan Trench. Holocene 18 (4), 517–528.
Schaff, D.P., Beroza, G.C., Shaw, B.E., 1998. Postseismic response of repeating aftershocks. Geophys. Res. Lett. 25 (24), 4549–4552.
Segall, P., Harris, R., 1987. The earthquake deformation cycle on the San Andreas fault near Parkfield, California. J. Geophys. Res. 92, 10511–10525.
Shibazaki, B., Matsuzawa, T., Tsutsumi, A., Ujiie, K., Hasegawa, A., Ito, Y., 2011. 3D modeling of the cycle of a great Tohoku-oki earthquake, considering frictional behavior at low to high slip velocities. Geophys. Res. Lett. 38 (21).
Shirzaei, M., Bürgmann, R., 2013. Time-dependent model of creep on Hayward fault inferred from joint inversion of 18 years InSAR time series and surface creep data. J. Geophys. Res., Solid Earth 118, 1733–1746. http://dx.doi.org/10.1002/jgrb.50149.
Shirzaei, M., Walter, T.R., 2010. Time-dependent volcano source monitoring using interferometric synthetic aperture radar time series: a combined genetic algorithm and Kalman filter approach. J. Geophys. Res. 115, B10421. http://dx.doi.org/10.1029/2010JB007476.
Shirzaei, M., Bürgmann, R., Taira, a, T., 2013. Implications of recent asperity failures and aseismic creep for time-dependent earthquake hazard on the Hayward fault. Earth Planet. Sci. Lett. 371–372, 59–66.
Simons, M., Minson, S.E., Sladen, A., Ortega, F., Jiang, J., Owen, S.E., Meng, L., Ampuero, J.P., Wei, S., Chu, R., Helmberger, D.V., Kanamori, H., Hetland, E., Moore, A.W., Webb, F.H., 2011. The 2011 magnitude 9.0 Tohoku-Oki earthquake: mosaicking the megathrust from seconds to centuries. Science 332 (6036), 1421–1425.
Uchida, N., Matsuzawa, T., 2013. Pre- and postseismic slow slip surrounding the 2011 Tohoku-oki earthquake rupture. Earth Planet. Sci. Lett. 374, 81–91.
Wang, K.L., Hu, Y., He, J.H., 2012. Deformation cycles of subduction earthquakes in a viscoelastic Earth. Nature 484 (7394), 327–332.
Zhao, D., Huang, Z., Umino, N., Hasegawa, A., Kanamori, H., 2011. Structural heterogeneity in the megathrust zone and mechanism of the 2011 Tohoku-oki earthquake (M_w 9.0). Geophys. Res. Lett. 38 (17).